Simulation of Microstructure Development in Injection Molding of Engineering Plastics

JEONG S. YU,* ALAN H. WAGNER,† and DILHAN M. KALYON‡

Stevens Institute of Technology, Department of Chemistry and Chemical Engineering, Castle Point Hoboken, New Jersey 07030

SYNOPSIS

Mathematical models were developed to predict the various microstructural properties, including birefringence, residual stress, and density distributions, in the freely quenched compression molded samples as well as in the injection molded samples. To model the birefringence distribution in the injection molded samples, the BKZ type integral constitutive equation was employed to account for the nonisothermal stress relaxation, which takes place during the cooling stage of the molding cycle. The predicted birefringence agreed well with the experimental data near the mold walls. The residual stress distribution was modeled by the existing thermoelastic theory. The residual thermal stress distribution in the freely quenched samples was predicted very well by the model. However, the predicted residual thermal stresses in the injection molded samples were much larger than the measured ones. A phenomenological model to predict the density distribution in injection molded sample is proposed by including the effects of both cooling rate and the pressure on the density development. The predicted results agreed well with the experimental data.

INTRODUCTION

The various mechanical and optical properties of injection molded articles are strongly affected by the thermo-mechanical history to which they are exposed during the molding cycle and the resulting microstructure.[1] Various aspects of the microstructure, including orientation distribution, density distributions, and residual stress distributions, can be predicted with mathematical models of the injection molding process in conjunction with realistic material properties.[2-9] The most recent literature regarding the simulation of injection molding process was recently reviewed by Kamal et al.,[6] where a comprehensive model was also presented. However, there were very few attempts to model density distributions in the injection molded specimens,[10,11] despite the fact that density is known to correlate directly with the refractive indices. On the other hand, modelling of residual stress distribution originates from the modelling of tempering stress in quenched inorganic glasses. There are thermoelastic models[12-14] and linear viscoelastic models.[15-19] In general, the residual stress distributions in the injection molded parts are more complicated than in the freely quenched part because of the flow-induced stresses generated in the melt state and subsequently frozen-in the molded parts by the rapid cooling process in addition to the thermally induced stresses.

In the following, we have modelled various elements of the microstructure development, including optical anisotropy, that is, birefringence distributions, residual stress distribution, and density distributions of two engineering plastic resins: poly(ether imide) and poly(phenylene ether). The predicted results were compared with the experimentally determined distributions. Furthermore, to understand the effect of thermal history on the microstructure development in the absence of flow effect, the microstructures of the freely quenched samples were also experimentally characterized and compared with the modelling results based on the experimentally determined boundary condition for

* Present Address: Lucky Central Research Center, Daejeon, Chung-Nam, Korea.

† Present Address: American Cyanamid, Bridgewater, NJ 08807.

‡ To whom correspondence should be addressed.

Journal of Applied Polymer Science, Vol. 44, 477-489 (1992)
 CCC 0021-8995/92/030477-13$04.00

heat transfer. The measured heat transfer quantities were also compared with the result of the finite difference solution of the one dimensional, unsteady heat conduction equation.

MATERIALS

Two engineering resins, that is, an unmodified poly(2,6-dimethyl-1,4-phenylene ether), PPE, and a poly(ether imide), PEI, were employed in this study. The PEI resin was manufactured by General Electric, with number and weight average molecular weights of 12,000 and 30,000, respectively. Its glass transition temperature was determined as 215°C. The PPE resin employed in our study had number and weight average molecular weights of 20,000 and 48,000, respectively. Its glass transition temperature was measured as 205°C.

EXPERIMENTAL

The experimental techniques and data regarding the rheological characterization,[20] thermo-physical properties of the resins,[21-23] injection molding behavior,[21] microstructure and ultimate properties,[22,24] and density distributions[11,25] were reported in our earlier works. In the present work, the heat transfer conditions during quenching of a flat sheet of PEI sample, sandwiched between two supporting aluminum plates in the ice water, were additionally measured. The sample was initially kept at 244°C between the two temperature controlled heated plates, followed by quenching in ice water. The heat transfer rate and the contact temperature were measured as a function of time at the interface between the plastic surface and the supporting aluminum plate during the quenching experiment. A Microfoil heat flow sensor manufactured by RdF Co. was used to measure the heat flux. Two thermocouples and one heat flow sensor were placed at the interface between the plastic and the aluminum plates and they were connected to a Hewlett-Packard 3497A data acquisition unit.

MATHEMATICAL MODELING

Molecular Orientation

The model was set up, simplifying the flow kinematics in conjunction with rigorously determined and realistic material properties of PEI and PPE. The basic assumptions of the model are:

1. One dimensional momentum and heat transfer.
2. Isothermal fully developed flow during the filling stage.
3. The fountain flow at the flow front is neglected.
4. The packing stage is neglected.
5. Constant temperature at the wall; value determined from experimental studies.
6. Nonlinear viscoelastic stress relaxation commences immediately after the filling of the mold and the relaxation of shear stress and first normal stress difference can be approximated by the relaxation of stresses upon cessation of steady simple shear flow.

We have employed a BKZ-type integral constitutive equation[26,27] with double exponential type damping functions.[28-30] The damping function is the strain dependent term of the factorized memory function. This constitutive equation has the general form of:

$$\underline{\underline{\tau}} = \int_{-\infty}^{t} M_0(t, t')h(I_1, I_2)C^{-1}\,dt' \qquad (1)$$

where $M_0(t, t')$ is the Lodge's rubber-like liquid memory function, $h(I_1, I_2)$ is the damping function, C^{-1} is the Finger relative strain tensor, and I_1 and I_2 are the first and second invariants of the Finger strain tensor. The various material parameters associated with eq. (1) and the shear material functions derived from eq. (1) can be found elsewhere.[20] During the isothermal filling stage, fully developed flow is assumed. However, a frozen skin layer is formed adjacent to the mold wall during the filling process.[1] The formation of the skin layer should thus reduce the available cross-sectional area for flow. As proposed by Dietz, White and Clark,[7] the thickness of the instantaneously formed skin layer may be estimated by:

$$\delta = \frac{T_g - T_w}{T_m - T_w}(4\alpha t_c)^{1/2} \qquad (2)$$

where δ is the thickness of the skin layer, T_g is the glass transition temperature of the polymer, T_m and T_w are the melt temperature and the temperature at the mold wall, α is the thermal diffusivity of the polymer, and t_c is the contact time, defined by:

$$t_c = \frac{L_c - x}{U} \tag{3}$$

where x is the distance from the gate of the mold, L_c is the total length of the mold, and U is the average velocity of the melt in the x direction. During the filling stage the experimentally monitored flow rate Q is used in the equation of continuity:

$$2\int_0^h u_x\, dy = Q/W \tag{4}$$

where Q is the volumetric flow rate, u_x is the x-component velocity, which varies with y only, and h and W are half of the gap and width of the mold, respectively. The equation of motion with the lubrication approximation reduces to:

$$\frac{\partial P}{\partial x} = -\frac{\partial \tau_{yx}}{\partial y} = \frac{\partial}{\partial y}\left[\eta(\dot\gamma)\dot\gamma\right] \tag{5}$$

which is integrated once with respect to y, being discretized into the finite difference form:

$$u_j = -\frac{1}{\eta_j}\frac{\partial P}{\partial x}(j-1)(\Delta y)^2 + u_{j+1} \tag{6}$$

for nodes $1 < j < MY - 1$, with a no-slip boundary condition at the wall, that is, $u\ (j = MY) = 0$. By solving eqs. (4) and (6), the shear-rate distribution in the mold is computed at the end of filling, from which the distributions of shear stress and the first normal stress difference at the end of filling are determined. The isothermal filling stage is followed by the cooling stage, in which nonisothermal stress relaxation occurs. In order to accommodate the stress relaxation in conjunction with the nonisothermal cooling history, the linear viscoelastic memory function in eq. (1) was determined as in Refs. 32 and 33:

$$M_0(t, t') = \sum_{k=1}^{N} \frac{g_k}{\lambda_k(T_0)a_T(t')} \times \exp\left(\frac{-1}{\lambda_k(T_0)}\int_{t'}^{t}\frac{dt''}{a_T(t'')}\right) \tag{7}$$

where λ_k and g_k are the linear viscoelastic parameters and a_T is a temperature shift factor,[33,34] which changes all relaxation times in the same ratio, as temperature varies. Thus,

$$\lambda_k(T) = a_T(T)\lambda_k(T_0) \tag{8}$$

As a mathematical expression for the temperature shift factor, we adopt an Arrhenius relationship for temperatures above $T_g + 100°C$[33] and the WLF equation[34] for temperatures below $T_g + 100°C$:

$$a_T(T) = \exp\left(\frac{E_a}{R}\left(\frac{1}{T} - \frac{1}{T_0}\right)\right) \quad \text{for } T > T_g + 100°C \tag{9}$$

$$\log(a_T(T)) = -\frac{C_1(T - T_g)}{C_2 + (T - T_g)} \quad \text{for } T_g < T < T_g + 100°C \tag{10}$$

where E_a is the activation energy, R is the universal gas constant, T_0 is the reference temperature for the melt, and C_1 and C_2 are WLF constants. The activation energy, E_a, was evaluated to be 43.8 kcal/mol for PEI and 42.5 kcal/mol for PPE[20] from the temperature dependence of magnitude of the complex viscosity values determined at low frequency. A reference temperature, T_0 of 290°C was selected. The WLF constants, C_1 and C_2, are 17.44 and 51.6 K, respectively.[34] The unsteady shear flow material functions corresponding to the nonisothermal stress relaxation after cessation of isothermal steady shear flow are derived from eq. (1), combined with the temperature dependent memory function, eq. (7), yielding:

$$\eta^-(t, \dot\gamma) = \sum_{k=1}^{N}\lambda_k(T_m)g_k\exp\left\{-\int_0^t\frac{dt''}{\lambda_k(t'')}\right\} \times\left[\frac{f}{[1 + n_1\dot\gamma\lambda_k(T_m)]^2} + \frac{1-f}{[1 + n_2\dot\gamma\lambda_k(T_m)]^2}\right] \tag{11}$$

$$\psi_1^-(t, \dot\gamma) = 2\sum_{k=1}^{N}\lambda_k(T_m)^2 g_k\exp\left\{-\int_0^t\frac{dt''}{\lambda_k(t'')}\right\} \times\left[\frac{f}{[1 + n_1\dot\gamma\lambda_k(T_m)]^3} + \frac{1-f}{[1 + n_2\dot\gamma\lambda_k(T_m)]^3}\right] \tag{12}$$

The parameters n_1, n_2 and f are the material parameters in the damping function:

$$h(\gamma) = f\exp(-n_1\gamma) + (1-f)\exp(-n_2\gamma) \tag{13}$$

where γ is the shear strain. The rheological parameters in the employed constitutive equation are listed in Tables I and II.

The relevant equations for the unsteady-state heat transfer in the cooling process may be summarized as follows:

Table I Relaxation Time λ_k and Strength g_k at T = 290°C

	g_k	
λ_k	Poly(phenylene ether)	Poly(ether imide)
1.0 E − 04	2.316 E05	7.838 E05
1.0 E − 03	1.210 E05	3.340 E05
1.0 E − 02	8.025 E04	3.130 E05
1.0 E − 01	3.008 E04	1.599 E05
1.0 E + 00	3.804 E03	2.410 E04
1.0 E + 01	4.968 E02	9.031 E02

$$\rho C_p \frac{\partial T}{\partial t} = \frac{\partial}{\partial y}\left(k \frac{\partial T}{\partial y}\right) \tag{14}$$

$$\text{I.C. } T(0, y) = T_m \tag{15}$$

$$\text{B.C.'s } \frac{\partial T}{\partial y} = 0 \quad \text{at the center} \tag{16}$$

$$T(t, h) = T_w \quad \text{at the wall} \tag{17}$$

where ρ, C_p, and k are the density, specific heat, and thermal conductivity. Following Dussinberre,[35,36] eqs. (14)–(17) are applied to both the melt and the solid phases, whereby ρ, C_p, and k are functions of temperature as experimentally determined in this study. Thus, there is no need to consider the moving boundary condition. Since it is not possible to obtain an analytical solution to this set of equations, the finite difference method was employed to get an approximate solution for the temperature distribution. According to the explicit finite difference scheme, eq. (21) becomes:

$$T_{j,k+1} = T_{j,k} + \frac{\alpha(T_{j,k})\Delta t(T_{j+1,k} - 2T_{j,k} + T_{j-1,k})}{\Delta y^2} + D(T_{j,k})\Delta t\left(\frac{T_{j+1,k} - T_{j-1,k}}{2\Delta y}\right)^2 \tag{18}$$

where j and k are spatial and time nodal points, respectively, Δy and Δt are the corresponding increments, and $\alpha(T) = k(T)/\rho(T)C_p(T)$ and $D(T) = (1/\rho(T)C_p(T))(dk(T)/dT)$ are evaluated at the temperature, $T_{j,k}$. The first normal stress difference, $N_1(y)$ and the shearing stress $\tau_{12}(y)$, determined at the glass transition temperature, were then related to the birefringence $\Delta n = n_{11} - n_{22}$ through[7]:

$$\Delta n = C(T > T_g)(N_1 + 4\tau_{12}^2)^{1/2} \tag{19}$$

where $C(T > T_g)$ is the stress optical coefficient above the glass transition temperature.

Residual Thermal Stress

We have employed an existing thermoelastic theory, proposed by Mills,[13] to predict residual thermal stress distributions in the freely quenched compression molded and the injection molded samples. The theory assumes that the stress is free up to the solidification temperature and the polymer behaves as a linearly elastic solid as it cools below the solidification temperature. The stress in the i-th layer is calculated by

$$\sigma_i = \frac{E_i}{1-\nu}[e_i - \alpha_L(T_i - T_s)] = \frac{E_i}{1-\nu}\left[\frac{L - L_i}{L_i} - \alpha_L(T_i - T_s)\right] \tag{20}$$

where E_i denotes the Young's modulus corresponding to the i-th layer temperature T_i, ν is the Poisson's ratio, α_L is the linear thermal expansion coefficient in the solid state, and T_s is the solidification temperature. The L and L_i are the gauge length and reference length for i-th layer, respectively. The value of L varies as a function of time and is independent of the location. It is calculated from the equilibrium condition:

$$\sum_{i=1}^{m} \sigma_i b_i = 0 \tag{21}$$

where m counts the number of solidified layers and b_i is the thickness of the i-th layer. By substituting eq. (20) into eq. (21), one obtains

$$L = \frac{\sum_{i=1}^{m} E_i b_i [1 + \alpha_L(T_i - T_s)]}{\sum_{i=1}^{m} E_i b_i / L_i} \tag{22}$$

Table II Parameters in Double Exponential Type Damping Function

	Poly(phenylene ether)	Poly(ether imide)
f	0.1152	0.1791
n_1	0.0149	0.0662
n_2	0.5893	0.3229

When the solidification is complete, eqs. (20) and (22) are used to calculate the residual stress when $T_i = T_{room}$. In the present study, the solidification temperature T_s in the original work of Mills[13] was replaced by the glass transition temperature, which is a function of cooling rate and pressure as proposed in our earlier work[11]:

$$T_g(q_1, P_1) = T_g(q_0, P_0)(1 + \gamma' P_1) + \theta' \log(q_1/q_0) \quad (23)$$

where $T_g(q_1, P_1)$ is the glass transition temperature at the cooling rate q_1 and the pressure P_1 and $T_g(q_0, P_0)$ is the glass transition temperature at the reference cooling rate q_0 and the atmospheric pressure P_0. The two material constants, γ' and θ' can be determined as described in our earlier work.[11]

Density Distributions

The density distribution in freely quenched sample was modeled by the fictive temperature theory.[37,38] The fictive temperature is defined as the temperature at which the structure will be at equilibrium.[37] The fictive temperature, T_f is coupled with temperature history through the differential rate equation.

$$\frac{dT_f}{dt} = -\frac{T_f - T}{\tau_0 a_T} \quad (24)$$

where τ_0 is the volume retardation time and a_T is the time-temperature shift factor. The details can be found elsewhere.[11] The specific volume was calculated from the determined distribution of the fictive temperature by:

$$v(t) = v_0 - \alpha_1'(T_0 - T_f) - \alpha_g'(T_f - T) \quad (25)$$

where v_0 and T_0 are the initial specific volume and temperature of the polymer and α_1' and α_g' are the slopes of the linear portions of equilibrium liquid and the glass in the volume–temperature plot. Equation (24) was solved by the finite difference method in conjunction with the unsteady heat conduction equation.

To model the density distribution in the injection molded specimen, a phenomenological model was proposed in our earlier work.[11] The effect of cooling rate and the formation pressure on the glass transition temperature and the density was integrated in the proposed model. Here we report the final results of the derivation. The glass transition temperature and the density are presumably determined by the cooling rate and the pressure at the time of solidification. The glass transition temperature is calculated using eq. (23) and the final density distribution is determined from

$$\rho(q_1, P_1) = \frac{\rho(q_0, P_0)(1 + \kappa' P_1)}{1 + \rho_0(q_0, P_0)\Delta\alpha'\theta' \log(q_1/q_0)} \quad (26)$$

where $\rho(q_0, P_0)$ is the density at the reference cooling rate q_0, and the pressure P_0, $\rho(q_1, P_1)$ is the density at the condition of cooling rate q_1 and P_1, $\Delta\alpha'$ is the difference between α_1' and α_g', and κ' is the pressure induced densification rate or the pseudo-compressibility of the polymer, which originates from the work of McKinney and Simha.[39] The concept of pressure induced densification rate was used by Greener[10] in his phenomenological model to predict the density distribution of injection molded specimens. The final density distribution in the injection molded specimen was calculated from the experimental cavity pressure and the calculated temperature history. The detailed information on the derivation of eq. (26), the computation algorithm, and the experimental methods employed for the determination of the various material properties can be found elsewhere.[11] The various material properties are listed for PEI and PPE in Table III.

RESULTS AND DISCUSSION

Heat Transfer in Freely Quenched Specimens

The contact temperature, monitored as a function of time, is shown in Figure 1. The lines represent the results obtained from finite difference solutions of the one dimensional heat conduction equation

Table III Material Properties for PEI and PPE

	PEI	PPE
E [MPa]	3000	2700
α_L [m/m K]	3.3 $E-5$	5.2 $E-5$
ν	0.4	0.4
T_{go} [K]	488	478
ρ_o [kg/m^3]	1286.6	1072.5
θ' [K]	0.88	Not Available
γ' [MPa^{-1}]	4.84 $E-6$	5.59 $E-6$
α_1' [m^3/kg K]	3.7 $E-7$	4.86 $E-7$
α_g' [m^3/kg K]	7.7 $E-8$	1.4 $E-7$
$\Delta\alpha'$ [m^3/kg K]	3.0 $E-7$	3.4 $E-7$
κ' [MPa^{-1}]	3.9 $E-5$	5.4 $E-5$

Note: The above data were taken from references [11] and [21].

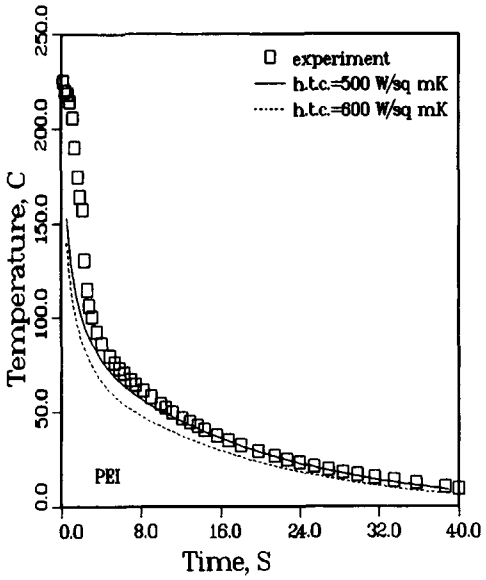

Figure 1 Comparison of experimentally determined contact temperature and calculated surface temperature for poly(ether imide) quenched from 244°C to 0°C in ice water.

[eqs. (14), (15), and (16)]. The convective heat transfer boundary condition at the plastic surface was used, instead of using eq. (17). The heat transfer coefficient in Figure 1 reflects the overall heat transfer coefficient, which is the sum of the three resistances, that is, the film heat transfer resistance at the interface between the plastic and the aluminum plate, thermal conductivity of the aluminum plate, and the film heat transfer resistance at the interface between the surface of the aluminum plate and the surrounding ice water. The value of heat transfer coefficient used in the numerical solution was determined from the measured heat flux and the temperature at the interface. The numerical results agreed well with the experimentally determined contact temperature.

In Figure 2, the experimentally obtained heat flux is shown as a function of elapsed time together with the numerical results. The heat flux at the surface of the plastic sample was calculated by utilizing the experimentally determined contact temperature history as a boundary condition at the surface. The computed results were again in good agreement with the experimental findings.

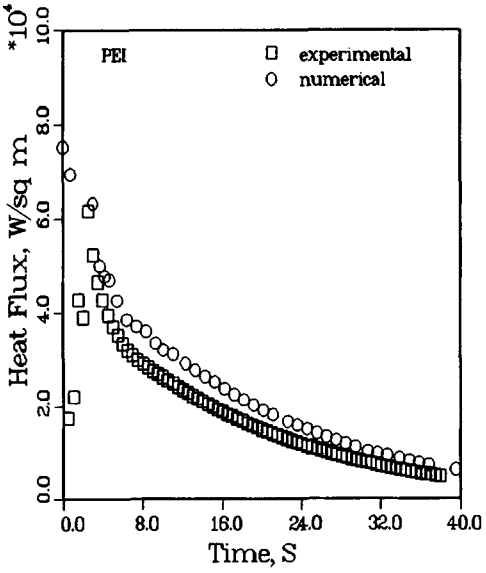

Figure 2 Comparison of experimentally and numerically determined heat transfer rates for poly(ether imide) quenched from 244°C to 0°C in ice water.

Microstructure Development in Freely Quenched Specimens

The experimentally determined distribution of the residual thermal stresses in the quenched specimen

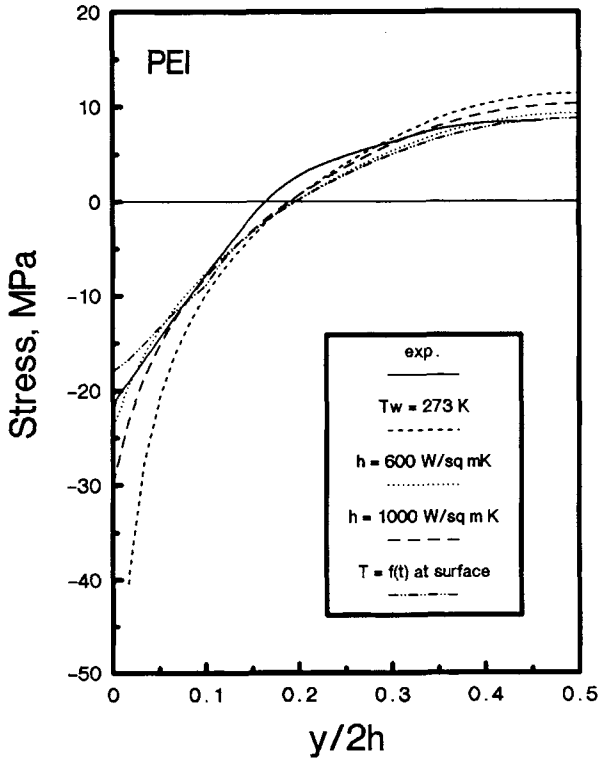

Figure 3 Comparison of experimental residual stress distribution with predictions from the thermoelastic theory for poly(ether imide) quenched from 250°C to 0°C in ice water.

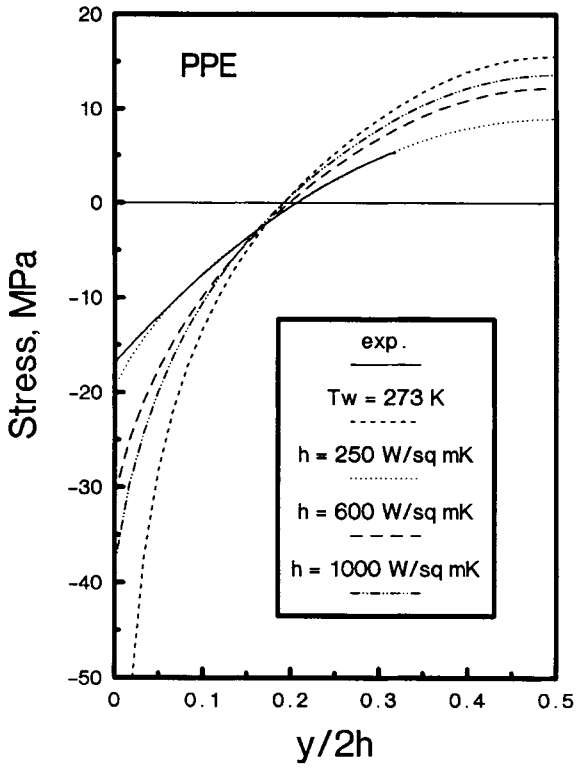

Figure 4 Comparison of experimental residual stress distribution with predictions from the thermoelastic theory for poly(phenylene ether) quenched from 230°C to 0°C in ice water.

of PEI is compared with the simulation results obtained for various heat transfer boundary conditions, as shown in Figure 3. Both the measured and predicted stress distributions were parabolic: compressive, and large at the surface and tensile, but less in the core region. For PEI, the experimental result is in excellent agreement with the computed result when the experimentally determined contact temperature is used and when the constant value of heat transfer coefficient, 600 W/sq K, is used. The residual stress distributions in quenched PPE specimen is shown in Figure 4. Good agreement between the experimental and the numerical results was seen for the heat transfer coefficient of 250 W/sq m K. The heat transfer resistances for both PEI and PPE, in the case of quenching in ice water, are expected to be similar. However, the lower heat transfer coefficient value provided the best fit for the PPE data. This may be due to the higher value of linear thermal expansion coefficient of PPE taken from the literature,[40] that is, 5.2 E-5 m/m K compared to that of PEI, that is, 3.3 E-5 m/m K, which was determined from dilatometry in our earlier work.[25]

The birefringence distributions in the quenched PEI and PPE sheets were measured using a wedge based technique as described elsewhere.[21,22] In Figures 5 and 6, the measured birefringence distributions are compared with the calculated birefringence distributions, which were obtained by the product of the stress optical coefficient determined at the room temperature and the residual stress. The confidence intervals (95%) are also shown. Small differences were observed between the measured and the predicted birefringence values. This may be due to the constant stress optical coefficient value used in the linear stress optical rule.

The gapwise density distribution in the quenched specimens of compression molded PEI and PPE are shown in Figures 7 and 8. The experimental results revealed that there are significant differences in the trends of density distributions of the quenched PEI and PPE samples. It is interesting to note that there are contradictory data reported in the literature on the gapwise density distributions of the freely quenched specimens of various resins.[41-44] The employed theory predicted lower density at the surface and higher density in the core as is the case for PEI. However, higher density values were observed at the surface and lower density values in the core of the

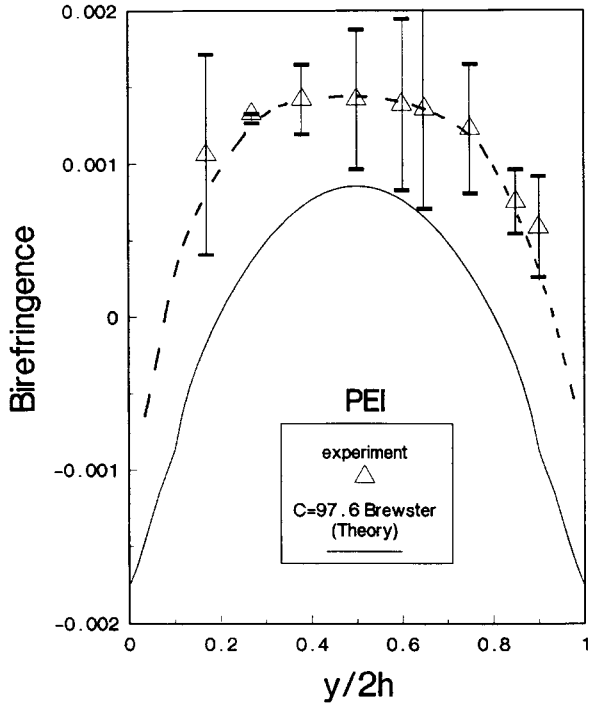

Figure 5 Comparison of the experimental birefringence distribution with the theoretical prediction for poly(ether imide) quenched from 250°C to 0°C in ice water.

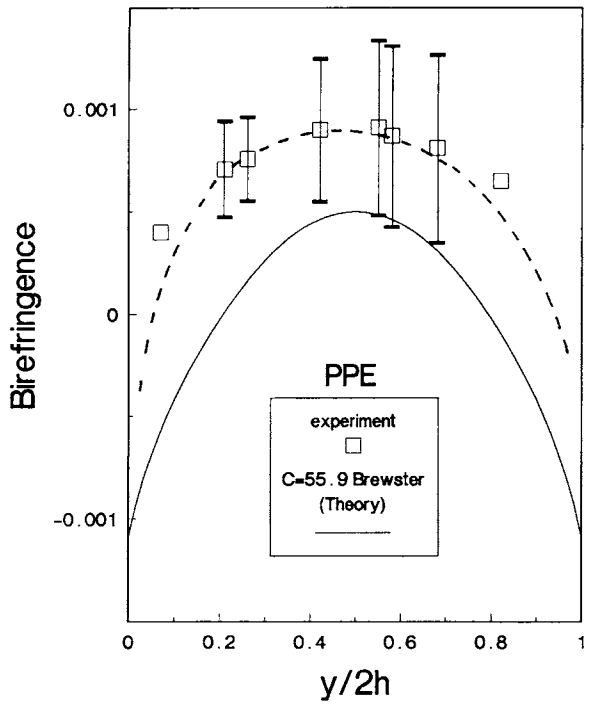

Figure 6 Comparison of the experimental birefringence distribution with the theoretical prediction for poly(phenylene ether) quenched from 230°C to 0°C in ice water.

quenched specimens of PPE. The employed theory can not predict the behavior of PPE. This may be due to the effect of thermal stresses being present in the sample. The surface layer is under compressive stresses, which may impart higher density. The experimental results suggest that there is a competition between the effects of the cooling rate and thermal stresses on the development of density in the freely quenched samples. The competing effects of cooling rate and the stress will be covered again in the discussion of density distributions of injection molded samples.

Microstructure Development in Injection Molded Specimens

The injection molding conditions used are listed in Table IV. Typical residual stress distributions, as determined experimentally by the layer removal technique, are shown in Figures 9 and 10. The samples are under compressive stresses at the surface and under tensile stresses in the core. Similar residual stress profiles have been observed for poly(sulfone)[45] and modified poly(phenylene oxide).[46] As seen in Figures 9 and 10, large differences exist between the measured residual stresses and the es-

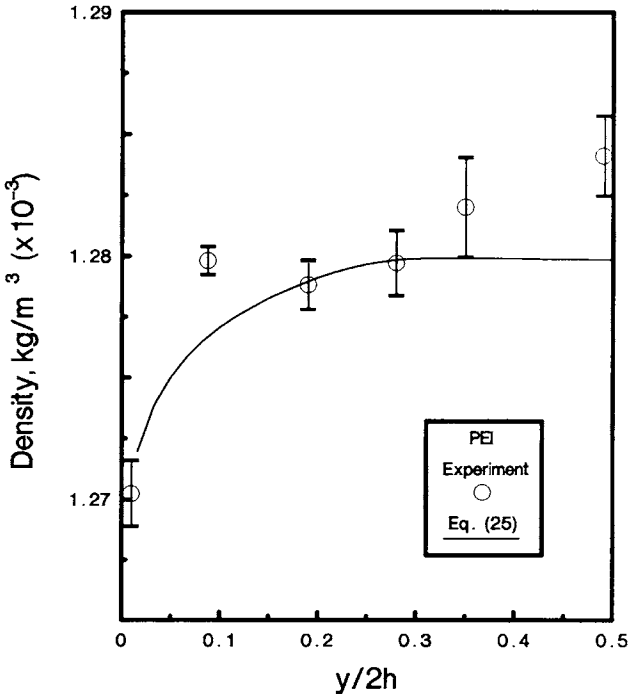

Figure 7 The experimental density distribution and the best fit of the theory for poly(ether imide) quenched from 300°C to 0°C in ice water.

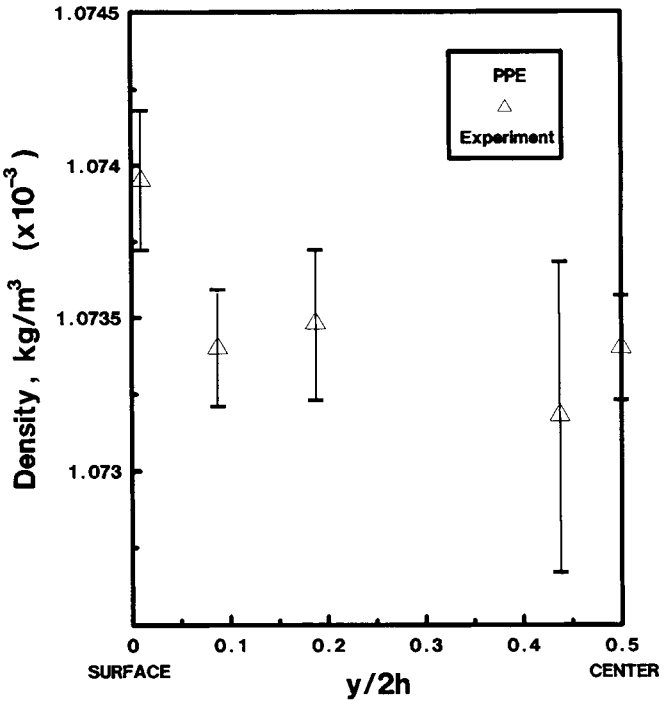

Figure 8 The experimental density distribution of poly(phenylene ether) quenched from 230°C to 0°C in ice water.

timated residual thermal stresses obtained with reasonable values of the heat transfer coefficient. According to Siegmann et al.,[45] the residual stresses in the injection molded sample are the result of not only the thermal stresses but also the flow induced stresses. The flow induced stresses are tensile in nature over the entire cross section, but the thermal stresses are compressive at the surface and tensile in the core. Therefore the superposition of these two stresses will result in lower compressive stresses at the surface as a result of the frozen-in flow induced stresses. In Figure 11, the sum of the shear stress and the first normal stress difference calculated at the end of cooling stage is shown for the two resins. The estimated stress values at the surface were negligibly small in comparison to the estimated thermal stresses. Therefore the measured residual stress distributions can not be quantitatively explained by the foregoing argument. A more comprehensive model is required in this area.

The birefringence distributions observed in the injection molded specimens reflect two different sources of molecular orientation. One is the flow induced molecular orientation brought about by the applied stress field and the other is the optical anisotropy caused by the thermal stresses, generated as a result of the rapid, inhomogeneous cooling condition. Figures 12 and 13 compare the typical theoretical predictions and experimental measurements of birefringence for the two resins. The experimental results and predictions agree near the mold wall. The model, however, predicts zero birefringence at the center of the sample while experimental data indicate positive birefringence. The birefringence

Table IV Processing Conditions Used in Injection Molding

Run #	Material	Screw Vel. (m/s)	Melt Temp. (°C)	Mold Temp. (°C)	Shot Size (in)
10	PPE	0.1	340	120	2.25
11	PPE	0.1	340	105	2.25
14	PEI	0.025	370	105	2.35
15	PEI	0.1	370	105	2.10

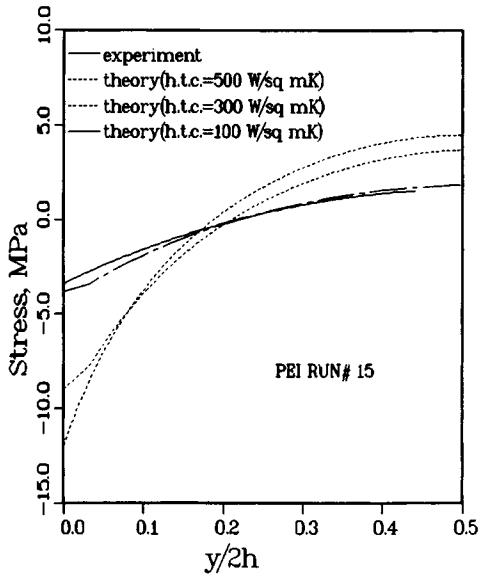

Figure 9 Residual stress distribution in the injection molded poly(ether imide) compared with the predicted thermal stress distribution.

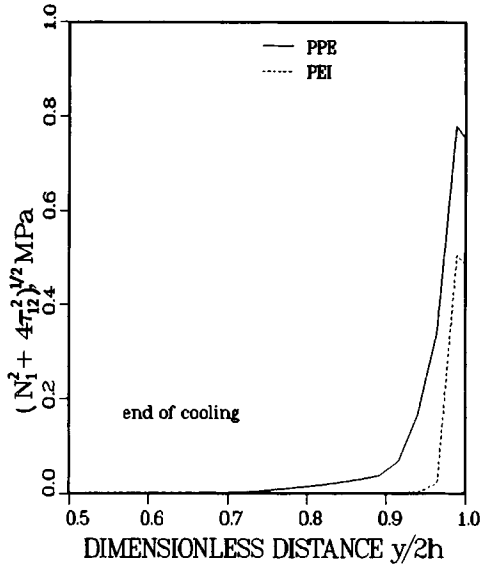

Figure 11 Typical comparison of the relaxation behavior of the combined shear stress and first normal stress difference for PPE and PEI (values determined at the end of cooling stage).

predicted by the model depends on the shear stress and the first normal stress difference. In the core of the sample, the shear stresses during the filling stage are very low, identically zero at the center. Furthermore, since the core region stays warmer longer than the skin region, more time is available for the macromolecules to relax. Hence the model predicts very low birefringence in the core region. The experimental birefringence values observed in the core can thus be attributed to unrelieved, thermally induced stresses, which the current model does not take into account.

The rapidly changing temperature and the pressure history experienced by the resin in the cavity

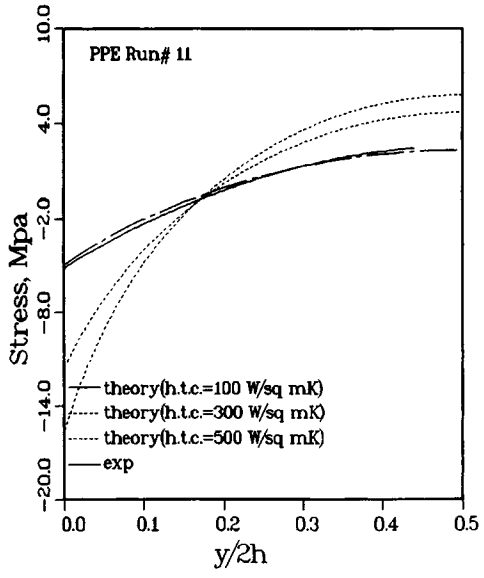

Figure 10 Residual stress distribution in the injection molded poly(phenylene ether) compared with the predicted thermal stress distribution.

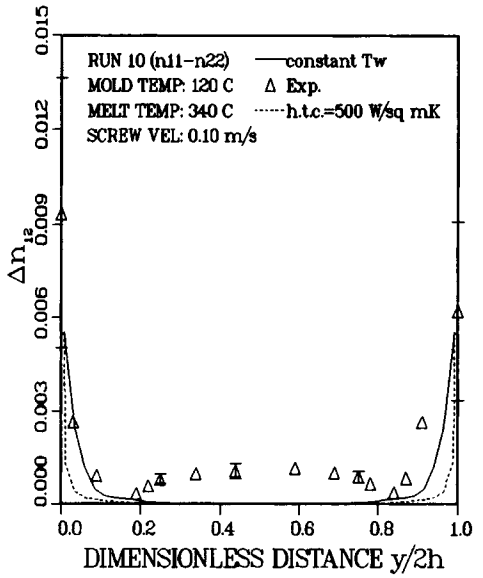

Figure 12 Typical comparison of the experimental birefringence distribution with the prediction for injection molded poly(phenylene ether).

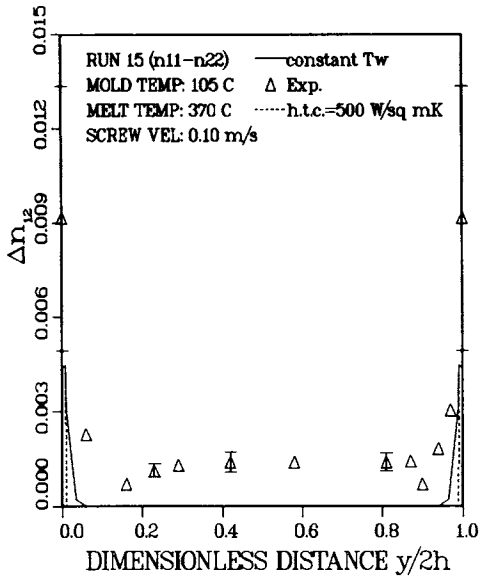

Figure 13 Typical comparison of the experimental birefringence distribution with the prediction for injection model poly(ether imide).

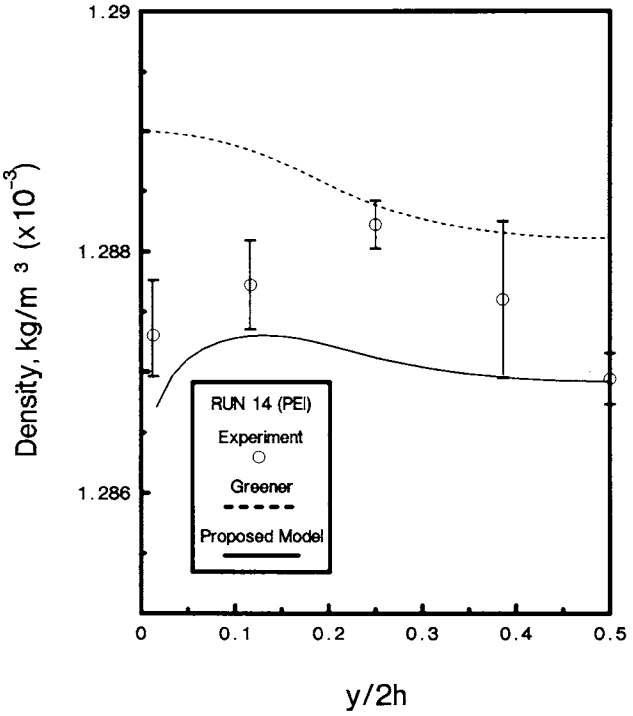

Figure 15 Typical comparison of the experimental density distribution with the prediction for injection molded poly(ether imide).

also results in the nonuniform density distributions. The surface region solidifies under the higher pressure and the higher cooling rate in comparison to the core region where the polymer solidifies at relatively lower pressures and cooling rates. The experimentally determined density distributions are shown for the two resins in Figures 14 and 15 with the 95% confidence interval. The trends are again different for the two resins. The injection molded PEI specimens exhibited low density values at the surface. Density increases to a maximum at about 750 μm away from the surface, then decreasing to a minimum value at the center. However, the injection molded PPE specimens exhibited a maximum density value at the surface. The density values monotonically decreased toward the core. Similar to the results with the freely quenched samples, the implication of these results is that the effect of pressure or stress on the density development is more pronounced for the injection molded PPE specimens. The pressure induced densification model proposed by Greener[10] was used to predict the density distribution of injection molded PPE. The predicted results agreed very well with the experimental results. However, the predictions of the Greener model, which neglects the effect of the cooling rate, were not as good for PEI especially at the surface region. This could be remedied by including the cooling rate

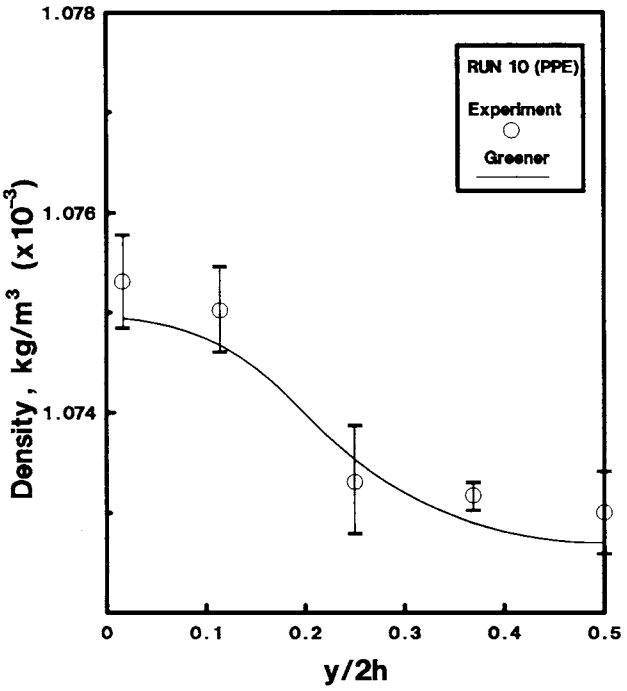

Figure 14 Typical comparison of the experimental density distribution with the prediction for injection molded poly(phenylene ether).

effect. The predictions from our densification model provided better agreement with the experimental results for PEI.

CONCLUSIONS

The various aspects of microstructure development in the injection molded specimens of two engineering thermoplastics, that is, poly(ether imide) and poly(phenylene ether) were investigated through mathematical modeling in conjunction with realistic material properties. Compressive stress values at the surface and tensile at the core were observed. The birefringence near the mold wall was fairly well predicted but the positive birefringence observed in the core region could not be predicted by the model. The birefringence in the core was attributed to the unrelieved portion of the thermally induced stresses. The density distribution in the injection molded specimens exhibited similar behavior as the quenched samples. The effect of pressure or stress on density development was more pronounced for PPE. A phenomenological model to predict the observed density behavior was proposed. Overall, the predicted density results were in good agreement with the experimental findings.

We gratefully acknowledge the financial support of the U.S. Army Research Office through Grant Number DAA L03-86-G-0048 and GE Corporation in terms of an unrestricted research grant.

REFERENCES

1. M. R. Kamal, D. M. Kalyon, and J. M. Dealy, *Polym. Eng. Sci.*, **20,** 1117 (1980).
2. M. R. Kamal and S. Kenig, *Polym. Eng. Sci.*, **12,** 302 (1972).
3. Z. Tadmor, *J. Appl. Polym. Sci.*, **18,** 1753 (1974).
4. M. R. Kamal, E. Chu, P. G. Lafleur, and M. E. Ryan, *Polym. Eng. Sci.*, **26,** 190 (1986).
5. H. Mavridis, A. N. Hrymak, and J. Vlachopoulos, *J. Rheol.*, **32**(6), 639 (1988).
6. M. R. Kamal, S. K. Goyal, and E. Chu, *AIChE J.*, **34,** 94 (1988).
7. W. Dietz, J. L. White, and S. Clark, *Polym. Eng. Sci.*, **18,** 273 (1978).
8. A. I. Isayev and C. A. Hieber, *Rheol. Acta,* **19,** 168 (1980).
9. J. Greener and G. H. Pearson, *J. Rheol.*, **27,** 115 (1983).
10. J. Greener, *Polym. Eng. Sci.*, **26,** 534 (1986).
11. J. S. Yu and D. M. Kalyon, *Polym. Eng. Sci.*, **31,** 153 (1991).
12. B. D. Aggawala and E. Saibel, *Phys. Chem. Glasses,* **2,** 137 (1961).
13. N. Mills, *J. Mat. Sci.*, **17,** 558 (1982).
14. D. G. LeGrand, *GE Technical Information Series,* Num. 85CRD127, July 1985.
15. E. H. Lee, T. G. Rogers, and T. C. Woo, *J. Amer. Cer. Soc.*, **48,** 480 (1965).
16. R. Gardon and O. S. Narayanaswamy, *J. Amer. Cer. Soc.*, **53,** 380 (1970).
17. S. M. Ohlberg and T. C. Woo, *J. Non-Crystalline Solids,* **14,** 280 (1974).
18. O. S. Narayanaswamy, *J. Amer. Cer. Soc.*, **61,** 146 (1978).
19. A. Markovsky, T. F. Soules, V. Chen, and M. R. Vukcevich, *J. Rheol.*, **31,** 785 (1987).
20. D. M. Kalyon, D. Yu, and J. S. Yu, *J. Rheol.*, **32,** 789 (1988).
21. A. H. Wagner, J. S. Yu, and D. M. Kalyon, *Adv. Polym. Techn.*, **9,** 17 (1989).
22. A. H. Wagner, J. S. Yu, and D. M. Kalyon, *Polym. Eng. Sci.*, **29,** 1298 (1989).
23. J. S. Yu, D. M. Kalyon, and A. H. Wagner, *SPE ANTEC Tech. Pap.*, **35,** 281 (1989).
24. A. H. Wagner, J. S. Yu and D. M. Kalyon, *SPE ANTEC Tech. Pap.*, **35,** 303 (1989).
25. J. S. Yu, M. Lim, and D. M. Kalyon, *Polym. Eng. Sci.*, **31,** 145 (1991).
26. M. H. Wagner, *Rheol. Acta,* **15,** 136 (1976).
27. M. H. Wagner and S. Stephenson, *J. Rheol.*, **23,** 489 (1979).
28. H. M. Laun, *Rheol. Acta,* **17,** 1 (1978).
29. K. Osaki, *Proceedings of the Seventh International Congress on Rheology,* C. Klason and J. Kubat, eds., Tages Anzeiger, Gothenburg, 1976, pp. 104–109.
30. R. B. Bird, R. C. Armstrong, and O. Hassager, *Dynamics of Polymeric Liquids,* Vol. 2, 2nd ed., Wiley, New York, 1987, Chap. 8.
31. M. Matsui and D. C. Bogue, *Trans. Soc. of Rheol.*, **21,** 133 (1977).
32. P. R. Soskey and H. H. Winter, *SPE ANTEC Technical Papers,* **28,** 47 (1982).
33. J. D. Ferry, *Viscoelastic Properties of Polymers,* 3rd ed., Wiley, New York, 1980, Chap. 11.
34. M. L. Williams, R. F. Landel, and J. D. Ferry, *J. Am. Chem. Soc.*, **77,** 3701 (1955).
35. G. Dussinberre, *Numerical Analysis of Heat Flow,* McGraw Hill, New York, 1949.
36. M. R. Kamal and D. M. Kalyon, *Polym. Eng. Sci.*, **23**(9), 503 (1983).
37. A. Q. Tool, *J. Am. Cer. Soc.*, **29,** 240 (1946).
38. R. O. Davies and G. O. Jones, *Proc. Roy. Soc., Ser. A.*, **217,** 26 (1953).

39. J. E. McKinney and R. Simha, *J. Res. Nat. Bur. Stand. Ser. A.*, **81,** 283 (1977).
40. A. Abolins, D. Aycock, and D. White, *Poly(phenylene ether)*, *Ency. Polym. Tech., VII,* GE, 1986, draft for publication.
41. J. Greener and P. M. Kenyon, *Proc. of SPIE,* San Diego, 1981.
42. A. I. Isayev and T. Hariharan, *Polym. Eng. Sci.*, **25,** 271 (1985).
43. A. Siegmann, A. Buchman, and S. Kenig, *Polym. Eng. Sci.*, **21,** 997 (1981).
44. F. H. Moy and M. R. Kamal, *Polym. Eng. Sci.*, **20,** 957 (1980).
45. A. Siegmann, S. Kenig, and A. Buchman, *Polym. Eng. Sci.*, **27,** 1069 (1987).
46. A. Siegmann, S. Kenig, and A. Buchman, *Polym. Eng. Sci.*, **21,** 997 (1987).

Received February 1, 1990
Accepted March 20, 1991